fluids

MDPI

Article

On the Modelling of Thermal Buoyancy Flows Involving Laminar–Turbulent Transition

Jingcheng Liu [1,2] and Xiangdong Li [3,*]

[1] School of China Alcoholic Drinks, Luzhou Technical College, Luzhou 620888, China; liujingcheng1980@126.com
[2] Key Laboratory of Liquor-Making Microbe Application and Measurement Technology of Luzhou, Luzhou 620888, China
[3] Department of Mechanical Engineering, The University of Melbourne, Parkville, VIC 3010, Australia
* Correspondence: xiangdong.li.1@unimelb.edu.au

Abstract

Laminar–turbulent transition is a phenomenon that extensively exists in many fluid flows. Accurate and cost-effective modelling of the transition is of fundamental importance for the design and diagnosis of relevant flow processes and industry systems. Existing transition turbulence models were mostly developed for high-speed aerodynamics applications. Their suitability for buoyant low-speed flows, such as natural and mixed convection flows, has been rarely assessed. This study aimed to bridge this gap through comparing the velocity and temperature fields yielded from various transition turbulence models against the experimental data of natural convection flow in a differentially heated cavity. The results showed that Wilcox's low-*Re* modification to the SST k-ω model and the transport γ-equation had good accuracies for low-speed natural convection flows. Other models, including the algebraic γ-equation, γ-Re_θ model and k_t-k_l-ω model, overpredicted the turbulence quantities, resulting in significant predictive errors in velocity and temperature simulations.

Keywords: laminar–turbulent transition; transition turbulence models; natural convection flow; model comparison; computational fluid dynamics

check for updates

Academic Editors: Yufeng Yao and Jun Yao

Received: 14 October 2025
Revised: 3 November 2025
Accepted: 4 November 2025
Published: 6 November 2025

Citation: Liu, J.; Li, X. On the Modelling of Thermal Buoyancy Flows Involving Laminar–Turbulent Transition. *Fluids* **2025**, *10*, 289. https://doi.org/10.3390/fluids10110289

Copyright: © 2025 by the authors. Licensee MDPI, Basel, Switzerland. This article is an open access article distributed under the terms and conditions of the Creative Commons Attribution (CC BY) license (https://creativecommons.org/licenses/by/4.0/).

1. Introduction

Laminar–turbulent transition in fluid flows is a phenomenon extensively encountered in many natural and industrial processes. The transition can happen in the boundary layer or free stream, as shown in Figure 1. The mechanisms of laminar–turbulent transition are highly complicated, involving many factors such as domain geometry, flow velocity, surface roughness, upstream disturbance, pressure gradient, heat input, etc., making their experimental characterization and theoretical modelling very challenging. Morkovin [1] was probably the first to investigate the mechanisms of transition in flow systems. He proposed that the transition can happen via multiple pathways, and these pathways can basically be classified into two types: natural transition and bypass transition. Natural transition is caused by small disturbances, which are progressively amplified as the fluid flows, leading to growing flow instabilities and ultimately full turbulence. On the other hand, bypass transition happens when the perturbations are sufficiently large, so that the natural transition is bypassed and the flow quickly becomes turbulent.

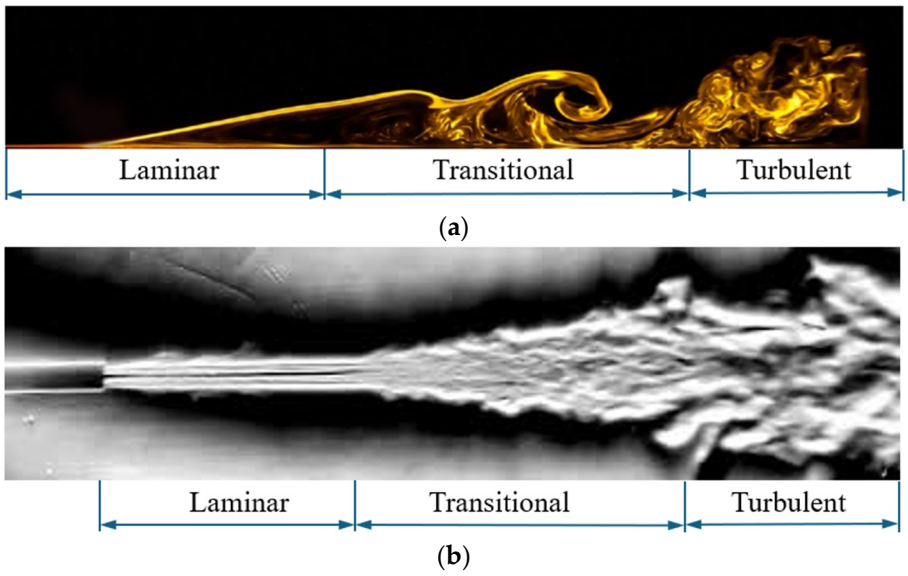


Figure 1. Flow visualization of the transition from laminar to turbulent flow: (**a**) laminar–turbulent transition in boundary layer flow [2]; (**b**) laminar–turbulent transition in jet flow [3].

The capability to predict and control flow transition is of fundamental importance for many engineering applications such as aircraft design, power generation, heating and cooling, material and chemical processing, etc. For this purpose, computational fluid dynamics (CFD) simulation is a commonly used tool. Given the time-dependent and anisotropic nature of laminar–turbulent transition, high-fidelity simulation techniques such as direct numerical simulation (DNS) and large eddy simulation (LES), both relying on fine spatial and temporal resolutions, are regarded as suitable for the depiction of the complex flow behaviors and promising for the mechanistic understanding of the associated flow physics. However, these methods are constrained by their prohibitive computational costs, especially when time and cost efficiencies are the priority. In contrast, Reynolds Average Navier–Stokes (RANS) models, in particular eddy viscosity models [4], offer a cost-effective alternative because they generally do not require high levels of spatial and temporal resolutions, making the analyses faster and cheaper. Eddy viscosity models are and will remain the workhorse of turbulence modelling at engineering scales for the foreseeable future.

However, conventional eddy viscosity models are based on the Boussinesq approximation that assumes turbulent eddies are isotropic. Theoretically, these models are only suitable for fully developed turbulent flows or turbulent eddies in the inertia and dissipation ranges in Kolmogorov's energy spectrum [5]. One key feature of transitional flows or flows in the transition region is that the flows are half-laminar and half-turbulent. To simulate transitional flows, these flow behaviors must be carefully formulated. Over the past decades, several transition turbulence models have been developed for this purpose. These models can be divided into two groups, namely, the "local-correlation-based" and "phenomenological" transition turbulence models, as shown in Figure 2.

Corrsin [6] introduced the intermittency factor γ ($0 \leq \gamma \leq 1$) to evaluate the fraction of time that the flow is turbulent at a specific spatial point, with $\gamma = 0$ indicating a fully laminar flow and $\gamma = 1$ for a fully turbulent flow. Corrsin's work laid the groundwork for the development of algebraic [7] and transport equations for γ [8], leading to a family of "local-correlation-based" turbulence models. In addition, Mayle and Schulz [9] introduced the concept of laminar kinetic energy k_l to describe the laminar fluctuations in the pre-transition region. They developed a transport equation for k_l, which was later

integrated into the k-ω model by Walters and Cokljat [10], resulting in a three-equation "phenomenological" k_t-k_l-ω turbulence model.

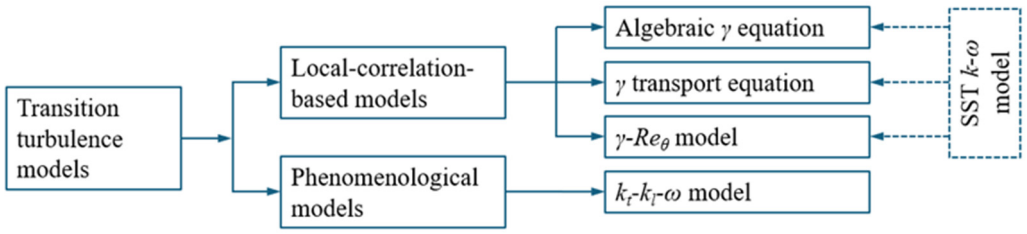


Figure 2. The classification of transition turbulence models.

These transition turbulence models were mostly developed for aerospace applications. They have been partially assessed for high-speed flows such as those over gas turbines [11,12] and airfoils [13,14]. However, their suitability for low-speed flows, especially natural convection or mixed convection flows where the buoyancy forces play a key role, has rarely been evaluated. Given the ubiquitousness of buoyancy flows in natural and industrial processes, it is crucial to develop or find a suitable turbulence model to improve their CFD simulations. In this study we aimed to bridge this gap by performing CFD simulations using various transition turbulence models. The simulated velocity and temperature fields were compared against experimental data reported in the literature. The results showed that Wilcox's low-*Re* modification to the SST k-ω model and the γ transport equation achieved good agreement with the experimental data. It should be noted that, strictly, Wilcox's low-*Re* modification is not a transition turbulence model; however, it achieved surprisingly good simulations for transitional flows. This attribute makes it a good option for engineering applications due to the low computational cost and good numerical stability. Comparatively, the γ transport equation offers a more mechanistic modelling at a slightly higher computational cost.

2. The Transition Turbulence Models

This study focused on thermal buoyancy flows of air with small temperature variations, such as those found in air-cooled electronics systems and occupied indoor spaces. This allowed us to ignore the density variation of the fluid and use the Boussinesq approximation to formulate thermal buoyancy forces. The mean flow was modelled using the RANS equations and air turbulence was modelled using the local-correlation-based and phenomenological transition turbulence models. The RANS equations have been elaborated elsewhere [4] and will not be repeated here for conciseness. The transition turbulence models are discussed as follows.

2.1. The Local-Correlation-Based Models

The local-correlation-based models are a group of transition turbulence models based on the intermittency factor γ, which can be modelled via an algebraic or transport equation. It should be noted that the γ-equation must be integrated into a suitable underlying turbulence model for a complete transition modelling. Various turbulence models have been used over the past decades, among which the SST k-ω model of Menter [15] is extensively used partially because it uses relatively fine mesh cells ($y^+ \approx 1$) to resolve the near-wall turbulence, enabling a more accurate depiction of flow transition. Within the SST k-ω framework, γ only modifies the production and dissipation terms of the k-equation, while the ω-equation and all other terms in the k-equation remain unchanged compared

to the SST k-ω model of Menter [15]. With the γ modification, the turbulence model is expressed by

$$\frac{\partial}{\partial x_i}(ku_i) = \frac{\partial}{\partial x_i}\left(\left(\nu + \frac{\nu_t}{\sigma_k}\right)\frac{\partial k}{\partial x_i}\right) + P_k^* - D_k^* + S_{k,b} \quad (1)$$

$$\frac{\partial}{\partial x_i}(\omega u_i) = \frac{\partial}{\partial x_i}\left(\left(\nu + \frac{\nu_t}{\sigma_\omega}\right)\frac{\partial \omega}{\partial x_i}\right) + P_\omega - D_\omega + D_{cd} + S_{\omega,b} \quad (2)$$

where k and ω are the turbulent kinetic energy and specific turbulence dissipation rate; u_i is the velocity component in the x_i coordinate axis; ν and v_t are the kinematic and turbulent kinematic viscosities; σ_k and σ_ω are the turbulent Prandtl numbers for k and ω; P_k^* and D_k^* are the modified production and dissipation terms for k; P_ω and D_ω are the production and dissipation terms for the specific turbulence dissipation rate ω; D_{cd} is the cross-diffusion term for ω.

$S_{k,b}$ and $S_{\omega,b}$ are buoyancy-induced source terms for k and ω, respectively, which are defined by

$$S_{k,b} = \beta g_i \frac{\nu_t}{Pr_t}\frac{\partial T}{\partial x_i} \quad (3)$$

$$S_{\omega,b} = \frac{\omega}{k}((1+\alpha)C_{3\varepsilon}S_{k,b} - S_{k,b}) \quad (4)$$

where α is an empirical constant and $C_{3\varepsilon}$ is a model constant.

The modified production and dissipation terms in the k-equation (Equation (1)) are expressed by, respectively,

$$P_k^* = \max(\gamma, \gamma_{sep})P_k \quad (5)$$

$$D_k^* = \min(\max(\max(\gamma, \gamma_{sep}), 0.1), 1.0)D_k \quad (6)$$

where P_k and D_k are the production and dissipation terms of k defined by Menter [15]. The above equations show that the modification is implemented via simply multiplying the original production and dissipation terms with the intermittency factor γ, which is then numerically bounded using a value associated with flow separation (γ_{sep}) in order to avoid unphysical behaviors.

The turbulent viscosity is calculated from k and ω yielded from the above turbulence model.

$$\nu_t = \frac{k}{\omega}\frac{1}{\max\left(\frac{1}{\alpha^*}, \frac{SF_2}{a_1\omega}\right)} \quad (7)$$

where α* and a_1 are empirical constants, S is the modulus of the strain rate tensor and F_2 is a blending function to smoothly bridge the k-ε and k-ω models.

The method to evaluate γ is different in different local-correlation-based models, as detailed below.

- The algebraic γ-equation

Algebraic equations are the simplest approach to the evaluation of γ. Equation (8) has been widely calibrated for external aeronautical flows.

$$\gamma = \tanh\left(Rat_{Re}^2\right) \quad (8)$$

where Rat_{Re} is the ratio of the empirical vorticity Reynolds number Re_{V22} to the critical momentum thickness Reynolds number $Re_{\theta C}$.

$$Rat_{Re} = \frac{Re_{V22}}{Re_{\theta C}} \quad (9)$$

$$Re_{V22} = \min\left(\frac{\max(S, \Omega, 0.1\omega)d_w^2}{2.2\nu}, 5000\right) \tag{10}$$

$$Re_{\theta C} = \min\left(\frac{210}{Tu_l}, 10000\right) FPG \tag{11}$$

where Ω is thcor, d_w is the distance to wall, Tu_l is the turbulence length scale and FPG is a function of pressure gradient.

- The γ transport equation

  Alternatively, γ can be modelled using a transport equation:

$$\frac{\partial \gamma}{\partial t} + \frac{\partial}{\partial x_i}(\gamma u_i) = \frac{\partial}{\partial x_i}\left(\left(\nu + \frac{\nu_t}{\sigma_\gamma}\right)\frac{\partial \gamma}{\partial x_i}\right) + P_\gamma - E_\gamma \tag{12}$$

where σ_γ is the turbulent Prandtl numbers for γ; P_γ and E_γ represent the production and elimination of γ due to the transition from laminar to turbulent flow and re-laminarization of turbulent flow, respectively.

$$P_\gamma = F_{length} S\gamma(1-\gamma)F_{onset} \tag{13}$$

$$E_\gamma = c_{a2}\Omega\gamma F_{turb}(c_{e2} - 1) \tag{14}$$

where F_{length} and F_{turb} are empirical functions; c_{a2} and c_{e2} are empirical constants. The laminar–turbulent transition is controlled by the onset condition F_{onset}, which is an algebraic function of the critical momentum thickness Reynolds number $Re_{\theta C}$ defined in Equation (11).

$$F_{onset} = f(Re_{\theta C}) \tag{15}$$

The exact expression of F_{onset} can be found elsewhere [16] and is omitted here for conciseness.

In the transport equation, the critical momentum thickness Reynolds number $Re_{\theta C}$ is expressed as an empirical algebraic equation of the boundary layer turbulence intensity and pressure gradient parameter. The algebraic expression significantly simplifies the calculation, which, however, may introduce errors and uncertainties.

- The γ-Re_θ model

To improve the γ transport equation, Langtry and Menter [17] developed an additional transport equation for the transition Reynolds number $R\tilde{e}_{\theta t}$, which was formulated based on the momentum thickness Reynolds number.

$$\frac{\partial R\tilde{e}_{\theta t}}{\partial t} + \frac{\partial}{\partial x_i}(R\tilde{e}_{\theta t}u_i) = \frac{\partial}{\partial x_i}\left(\sigma_{\theta t}(\nu + \nu_t)\frac{\partial R\tilde{e}_{\theta t}}{\partial x_i}\right) + P_{\theta t} \tag{16}$$

where $\sigma_{\theta t}$ is the turbulent Prandtl number for $R\tilde{e}_{\theta t}$. The production term of $R\tilde{e}_{\theta t}$ is defined by

$$P_{\theta t} = \frac{c_{\theta t}}{t}(Re_{\theta t} - R\tilde{e}_{\theta t})(1.0 - F_{\theta t}) \tag{17}$$

where $F_{\theta t}$ is an empirical coefficient. Equations (12) and (17) together constitute the γ-Re_θ model.

2.2. The Phenomenological k_t-k_l-ω Model

The phenomenological models use a different approach to the modelling of turbulence transition. Walters and Cokljat [10] proposed that the fluctuation behaviors in the pre- and post-transition regions are different, and therefore introduced the laminar kinetic energy k_l and turbulent kinetic energy k_t to evaluate the energy carried by the large-scale

(low-frequency) velocity fluctuations in the pre-transition boundary layer and small-scale (high-frequency) velocity fluctuations displaying the characteristics of fully turbulent flow. Correspondingly, the turbulent viscosity is divided into a large-scale and a small-scale component corresponding to k_l and k_t, respectively. The total fluctuation kinetic energy and total turbulent viscosity are the sum of the components.

$$k = k_t + k_l \tag{18}$$

$$\nu_t = \nu_{t,s} + \nu_{t,l} \tag{19}$$

Based on the k-ω model and Morkovin's [1] theory of natural and bypass pathways, Walters and Cokljat developed the following transport equations for k_l, k_t and ω, forming a 3-equation k_l-k_t-ω model.

$$\frac{\partial k_t}{\partial t} + \frac{\partial}{\partial x_i}(k_t u_i) = \frac{\partial}{\partial x_i}\left(\left(\nu + \frac{\alpha_t}{\alpha_k}\right)\frac{\partial k_t}{\partial x_i}\right) + P_{k_t} + R_{BP} + R_{NAT} - \omega k_t - D_{k_t} + S_{k_t,b} \tag{20}$$

$$\frac{\partial k_l}{\partial t} + \frac{\partial}{\partial x_i}(k_l u_i) = \frac{\partial}{\partial x_i}\left(\nu\frac{\partial k_l}{\partial x_i}\right) + P_{k_l} - R_{BP} - R_{NAT} - D_{k_l} + S_{k_l,b} \tag{21}$$

$$\begin{aligned}\frac{\partial \omega}{\partial t} + \frac{\partial}{\partial x_i}(\omega u_i) = \frac{\partial}{\partial x_i}\left(\left(\nu + \frac{\nu_t}{\sigma_k}\right)\frac{\partial \omega}{\partial x_i}\right) + C_{\omega 1}\frac{\omega}{k_t}P_{k_t} + \left(\frac{C_{\omega R}}{f_W} - 1\right)\frac{\omega}{k_t}(R + R_{NAT}) \\ -C_{\omega 2}\omega^2 + C_{\omega 3} f_\omega \alpha_t f_W^2 \frac{\sqrt{k_t}}{d_w^3} + S_{\omega,b}\end{aligned} \tag{22}$$

where α_k, α_t, $C_{\omega 1}$, $C_{\omega R}$, f_W, $C_{\omega 2}$, $C_{\omega 3}$, and f_ω are empirical constants. P_{k_t}, P_{k_l} and D_{k_t}, D_{k_l} are production and dissipation terms for k_t and k_l, respectively. $S_{k_t,b}$, $S_{k_l,b}$ and $S_{\omega,b}$ are source terms due to buoyancy. The key components in the k_l-k_t-ω model are the terms describing the production of turbulence due to the natural and bypass pathways, R_{NAT} and R_{BP}, expressed by

$$R_{NAT} = C_{R,NAT}\beta_{NAT} k_l \Omega \tag{23}$$

$$R_{BP} = \frac{C_R \beta_{BP} k_l}{f_W} \tag{24}$$

The production terms (P_{k_l} and P_{k_t}) and dissipation terms (D_{k_l} and D_{k_t}) of k_t and k_l are defined by, respectively,

$$P_{k_t} = \nu_{t,s} S^2 \tag{25}$$

$$P_{k_l} = \nu_{t,l} S^2 \tag{26}$$

$$D_t = 2\nu \frac{\partial \sqrt{k_t}}{\partial x_i}\frac{\partial \sqrt{k_t}}{\partial x_i} \tag{27}$$

$$D_l = 2\nu \frac{\partial \sqrt{k_l}}{\partial x_i}\frac{\partial \sqrt{k_l}}{\partial x_i} \tag{28}$$

2.3. Wilcox's Low-Reynolds Number Modification

Wilcox's low-*Re* modification [18] to the SST k-ω model in essence is not a transition turbulence model because it does not include any transition formulation. However, it has achieved surprisingly good accuracy for the simulation of high-speed transitional flows [7,19]. Therefore, it is included here to assess its suitability for low-speed thermal buoyancy flows.

According to Menter's definition [15], the coefficient a^* = 1 in the turbulent viscosity formula (Equation (7)), which makes the SST k-ω model mainly suitable for high-

Reynolds number flows. To simulate low-Reynolds number turbulent flows using the model, Wilcox [18] re-defined the coefficient as

$$a^* = a^*_\infty \left(\frac{a^*_0 + Re_t / R_k}{1 + Re_t / R_k} \right) \tag{29}$$

where Re_t is the turbulent Reynolds number; other parameters are all empirical constants. The modification potentially affects the laminar–turbulent transition process as it produces a delayed onset of the turbulent boundary layer and constitutes a very simple approach to the modelling of laminar–turbulent transition. Studies [7,19] using the low-*Re* modification achieved surprising successes for the simulation of transitional flows, which, however, were believed to be "accidental artifacts" [20]. Nevertheless, owing to the low computational cost and surprising accuracy, the SST k-ω model with Wilcox's low-*Re* modification is sometimes recommended as a useful option for transitional flows in engineering applications [10]. After all, the Boussinesq approximation that underpins the eddy viscosity models has been widely accepted and proven effective in engineering fields, although it is often criticized for lacking theoretical soundness.

3. Numerical Procedures

The experiments of natural convection flow of air by Salat et al. [21] were selected for model validation in this study. The experiments were performed in a differentially heated cubic cavity with dimensions of 1000 × 1000 × 1000 mm, as illustrated in Figure 3a. Two opposite vertical walls (low-X and high-X walls) were maintained at constant temperatures through water circulation. The hot wall had a temperature of T_h = 30 °C and the cold wall had a temperature of T_c = 15 °C. The cavity was divided into 3 chambers, where the middle chamber (320 mm thickness) was the test chamber and the side chambers served as thermal guards. This configuration made the side walls of the test chamber near-adiabatic. The top and bottom walls were insulated using polyurethane foam and their temperature was monitored using T-type thermocouples. The test chamber had a Rayleigh number of 1.5×10^9 [21], indicating the natural convection flows in it were in the range of laminar–turbulent transition [22]. Temperature and velocity measurements of air in the test chamber were performed using thermocouples and a laser Doppler anemometer along a 60 mm horizontal line (Test line 1) at a height of 500 mm and a 500-mm vertical line (Test line 2) in the middle plane of the test chamber. Test lines 1 and 2 represented a near-wall region and broader region, covering both the near-wall and bulk regions.

The test chamber was selected as the computational domain, which was then discretized using a structured mesh, as shown in Figure 3b. Local mesh refinement was applied in near-wall regions, resulting in $y^+ < 0.11$ on all solid surfaces, which ensured sufficient boundary layer resolutions. Mesh independence was achieved at 2.8 million cells, as a further mesh refinement by a factor of 1.3 in all coordinate directions following the procedure recommended by Celik et al. [23] only caused a small change (<0.5%) in the air velocity profiles along a vertical test line, as shown in Figure 4. Constant temperatures were applied at the hot, cold, top and bottom walls according to the experimental condition, while the side walls were treated as adiabatic. A total of 5 computational cases, each with a different transition turbulence model, were completed, as listed in Table 1. The above model equations together with the RANS equations were discretized using the finite volume method with the 2nd-order upwind scheme and solved using the coupled solver built in the commercial CFD code Ansys Fluent 2024R2. Being different from the segregated algorithms such as the SIMPLE and PISO algorithms, the coupled solver solves the continuity and momentum equations in a coupled way, and then solves the energy and

turbulence equations in a segregated way, enabling a fast convergence. Convergence was achieved within 5000 iterations when all residuals dropped below 1×10^{-4}.

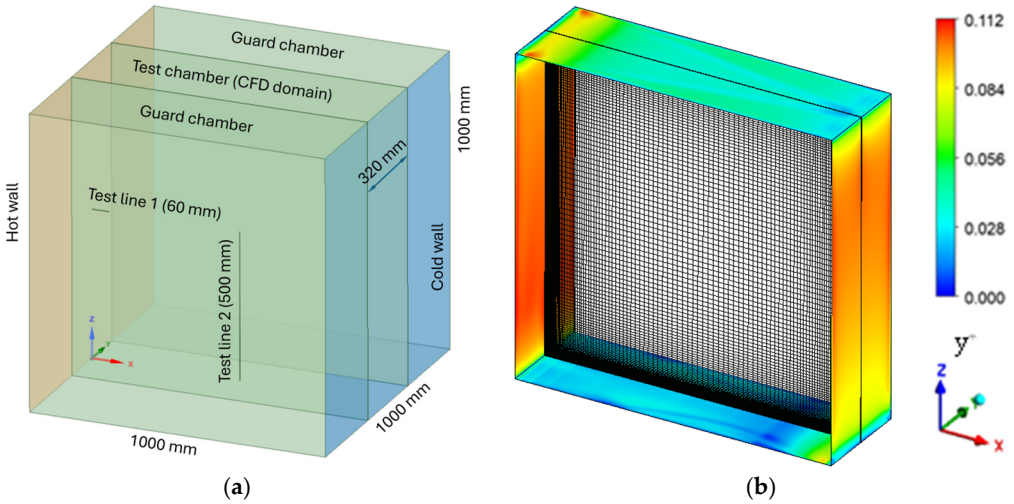


Figure 3. The geometry model and computational mesh of this study: (**a**) the experimental chamber of Salat et al. [21]; (**b**) mesh details and y^+.

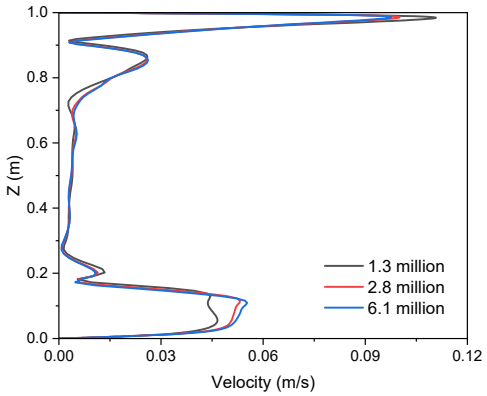


Figure 4. Mesh independence analysis.

Table 1. Computational cases with different transition turbulence models.

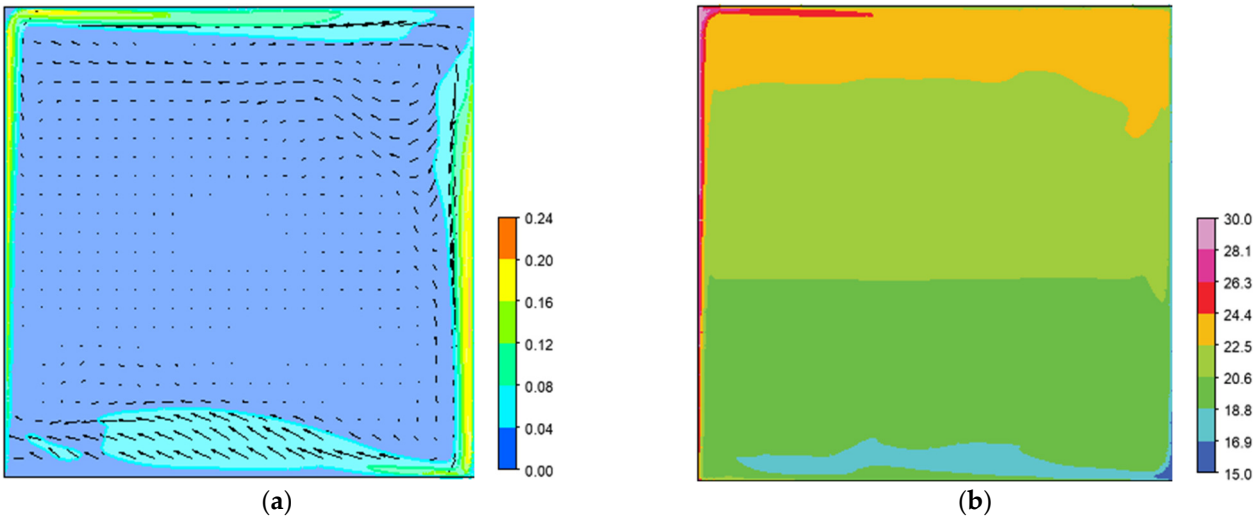
Case No.	Turbulence Model
1	SST k-ω model with algebraic γ-equation
2	SST k-ω model with transport γ-equation
3	SST k-ω model with γ-Re_θ model
4	k_t-k_l-ω model
5	SST k-ω model with Wilcox's low-Reynolds number modification

4. Results and Discussion

4.1. Air Velocity and Temperature Fields

The simulations showed that driven by the thermal buoyancy forces, naturally circulating flows and thermal stratification are formed in the test chamber. Figure 5a,b show the typical air velocity and temperature contours in the middle plane (Y = 0 m), respectively. The figure shows that the air next to the hot wall was heated up, forming a rising flow in the vicinity of the hot wall. The flow then changed to the horizontal direction upon

approaching the ceiling. The temperature and velocity of the horizontal flow gradually decreased as it moved towards the cold wall while keeping attached to the ceiling. The flow then turned downwards as it reached the cold wall. However, the air at this position had a higher temperature and hence a lower density than that at lower heights, the buoyancy force drove a part of the descending flow to change its direction and move horizontally towards the hot wall. The strength of the horizontal flows gradually reduced as the temperature of the air decreased. Significant descending flow was observed next to the cold wall, which turned into a cold, horizontal flow towards the hot wall at the bottom of the cavity. The stratified horizontal flows were a key factor contributing to steady thermal stratification in the cavity (Figure 5b).



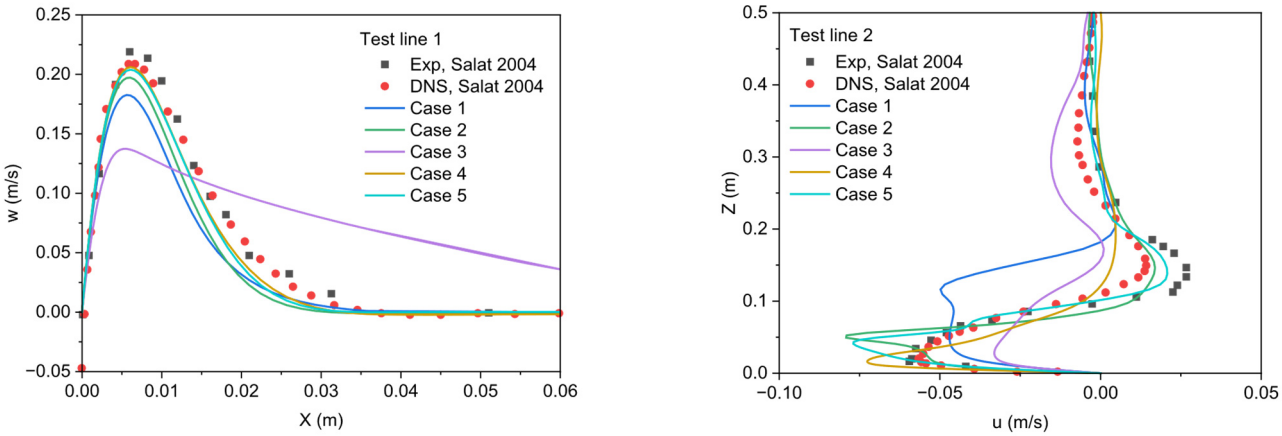
(**a**) (**b**)

Figure 5. Contours of simulated air velocity and temperature in the plane Y = 0.0 m (Case 1): (**a**) velocity (m/s); (**b**) temperature (°C).

The air velocity and temperature distribution patterns yielded from the transition turbulence models described in Section 2 were qualitatively similar. However, quantitatively, these models produced different air velocity and temperature fields, indicating different capabilities of turbulence modelling resulting in different heat transfer and flow simulations. The simulated profiles of w-velocity along the short horizontal line (Test line 1) and u-velocity along the longer vertical line (Test line 2) in Figure 1 are compared against their corresponding experimental data in Figure 6a and b, respectively. The DNS data by Salat et al. [21] are also included in the figure. Figure 6a shows that all turbulence models predicted that the magnitude of the w-velocity quickly increased from the wall, then peaked at a position approximately 5–8 mm from the wall before decreasing towards the cavity center. Quantitatively, most transition turbulence models except the γ-Re_θ model (Case 3) achieved good agreement with the experimental data and DNS simulation in the near-wall regions. In a larger region (Test line 2, shown in Figure 6b), the γ transport equation (Case 2) and Wilcox's low-Re modification (Case 5) performed best, especially in the regions of Z < 0.2 m.

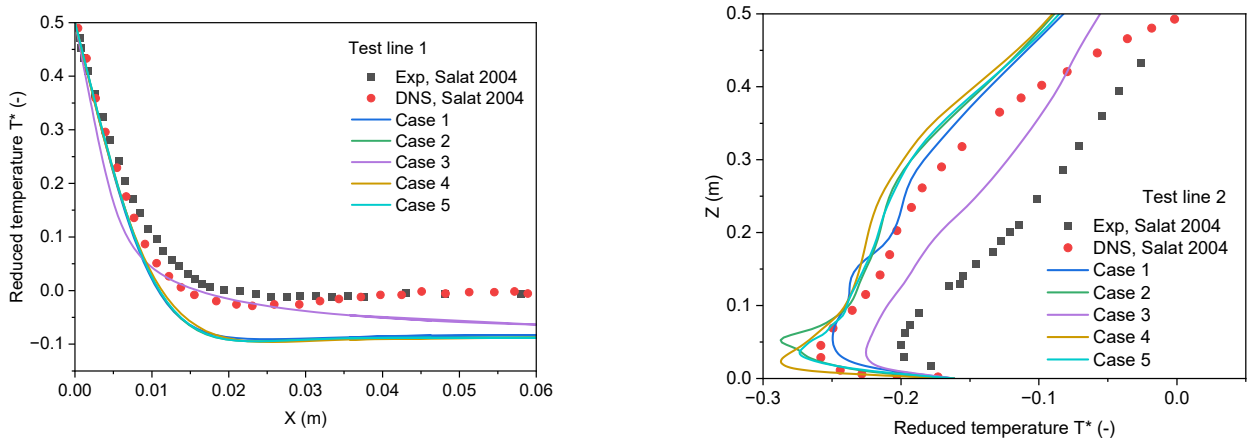
Correspondingly, the simulated air temperature profiles along the test lines are compared against the experimental data in Figure 7, where the dimensionless reduced temperature is defined by

$$T^* = \frac{T - (T_h + T_c)/2}{T_h - T_c} \tag{30}$$



(**a**) (**b**)

Figure 6. Comparison of simulated air velocity against experimental data [21]: (**a**) Test line 1; (**b**) Test line 2.



(**a**) (**b**)

Figure 7. Comparison of simulated air temperature against experimental data [21]: (**a**) Test line 1; (**b**) Test line 2.

Compared to the velocity simulation, the agreement between the CFD results and experimental data of air temperature was not great, suggesting some experimental details may not have been fully taken into account in the CFD models (for example, actual temperature distribution on the cold and hot walls, surface roughness, disturbance to the flow field by thermal couples, etc. could not be fully considered in the CFD model). However, the temperature profiles yielded from the transition turbulence models basically matched the DNS data of Salat et al. [21], which indicated the reliability of the numerical simulations of this study. Figure 7 shows that the agreement was very good in the near-wall regions (X < 0.01 m for Test line 1 and Z < 0.2 m for Test line 2). However, deviations were observed in the regions away from the walls. Among all the investigated models, the γ transport equation (Case 2) and Wilcox's low-*Re* modification (Case 5) had the best, though comparable, accuracies, while the γ-Re_θ model (Case 3) was the least accurate.

4.2. Effects of Turbulence Modelling on Flow and Heat Transfer Simulations

The above deviations in air velocity and temperature simulations were strongly related to the method of turbulence modelling used by different models. The investigated cavity of this study did not have an inlet or outlet for air supply or exhaust; thus, the air flow was purely driven by thermal buoyancy forces. As a result, the air turbulence only resulted

from the thermal buoyancy flows. When different turbulence models were used, different degrees of air turbulence were predicted, which then affected the simulations of air velocity, temperature, etc. To help understand the strength of turbulence yielded from different turbulence models and their effects on the mean flow and heat transfer, the eddy viscosity ratio ν_r, defined as the ratio of the turbulent viscosity to the kinematic viscosity of the fluid ($\nu_r = \nu_t/\nu$), was plotted in Figure 8 for the plane of Y = 0 m. The turbulent viscosity ratio represented the relative strength of the turbulent viscosity compared to the molecular viscosity of air, and therefore can be used as an indicator of turbulence strength. A ν_r value smaller than 1.0 indicated that the local shear stress in the flow was mainly due to the molecular viscosity of the fluid, while $\nu_r > 1$ meant turbulent fluctuations played a dominant role in generating the shear stress. The curves of $\nu_r = 1$ were extracted and added in Figure 8 (black curves) to illustrate the laminar- and turbulence-dominated regions.

The results show that the low-*Re* modification (Case 5) produced the lowest ν_r values throughout the domain, followed by the γ transport equation (Case 2), as shown in Figure 8e and b, respectively. Both models predicted that the flow in the cavity was near-laminar, only with small areas having $\nu_r > 1.0$. In addition, the simulations showed that the local-correlation-based models performed very differently than the phenomenological model in terms of turbulent viscosity. Figure 8a,c show that both the algebraic γ-equation (Case 1) and γ-Re_θ model (Case 4) predicted that the near-wall regions would have a large turbulent viscosity ratio, while the bulk region in the middle of the cavity is dominated by laminar flows. However, the k_l-k_t-ω model produced a very different ν_r distribution pattern indicating that most of the cavity was dominated by turbulent flows, while only the boundary layers were controlled by laminar flows. Moreover, the k_l-k_t-ω model predicted a significantly thicker boundary layer than the γ-based models.

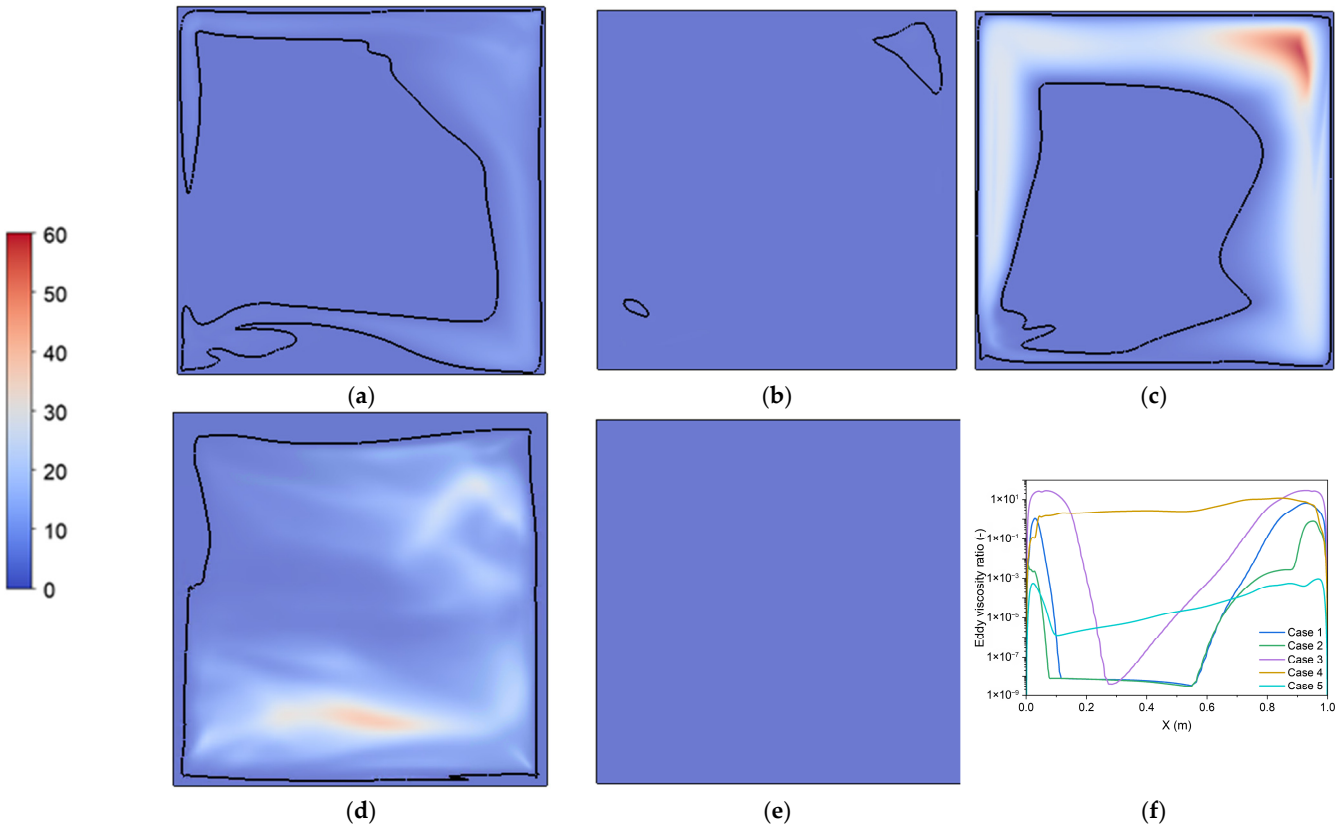


Figure 8. The contour plots of turbulent viscosity ratio in the plane of Y = 0 m (note: the black curves in the contours represent the turbulent viscosity ratio $\nu_r = 1$): (**a**) Case 1; (**b**) Case 2; (**c**) Case 3; (**d**) Case 4; (**e**) Case 5; (**f**) ν_r profiles.

A quantitative comparison of the turbulent viscosity ratio along the horizontal line at Z = 0.5 m in the Y = 0 plane is presented in Figure 8f. The figure shows that the line can basically be divided into three regions: near-wall regions next to the hot (X < 0.2 m) and cold (X > 0.8 m) walls, and the bulk region sitting between the near-wall regions. The results show that the low-*Re* modification (Case 5) produced the lowest eddy viscosity in the near-wall regions, followed by the γ transport equation (Case 2), while the γ-Re_θ model (Case 3) produced the largest eddy viscosity in these regions. The predicted maximal and minimal eddy viscosity was more than 1000 times apart, and this was believed to be the main cause of the lowest air rising velocity in the near-wall regions produced by the γ-Re_θ model, as shown in Figure 6a. In the bulk region (0.2 m < X < 0.8 m), however, the k_l-k_t-ω model (Case 4) produced the highest turbulent viscosity, which was 2 to 11 times the kinematic viscosity of air and more than 100 times that produced by the algebraic γ-equations and γ transport equation. This explained the lowest air velocity (Figure 6b) and highest reduced temperature (Figure 7b) simulated by the k_l-k_t-ω model.

To further assess the models' capabilities of modelling flow transition, the contours of intermittency (γ) in the plane of Y = 0 m were plotted, as shown in Figure 9, for the local-correlation-based models (Cases 1–3). According to the definition of the intermittency, γ = 0 meant the flow was fully laminar, while γ = 1 represented fully turbulent flow. As shown in Figure 9a, the algebraic γ-equation predicted that laminar flow mainly existed in the boundary layers and a region in the center of the cavity, while turbulent flows existed in a close loop region. Comparatively, the region next to the cold wall had a stronger turbulence intensity than that next to the hot wall. The transport γ-equation, on the other hand, predicted that turbulent flow only existed in two opposite cavity corners, sitting at the beginning points of the hot and cold walls, while all other regions are dominated by laminar flow, as shown in Figure 9b. The γ-Re_θ model predicted that almost the entire cavity except the boundary layers was dominated by turbulent flow, as shown in Figure 9c. As the flow in the cavity was purely driven by thermal buoyancy force, and given the discrepancies between the predicted air velocity and temperature as shown in Figures 6 and 7, we suspected that the level of turbulence was overpredicted by the algebraic γ-equation and γ-Re_θ model. Comparatively, the transport γ-equation produced the best prediction.

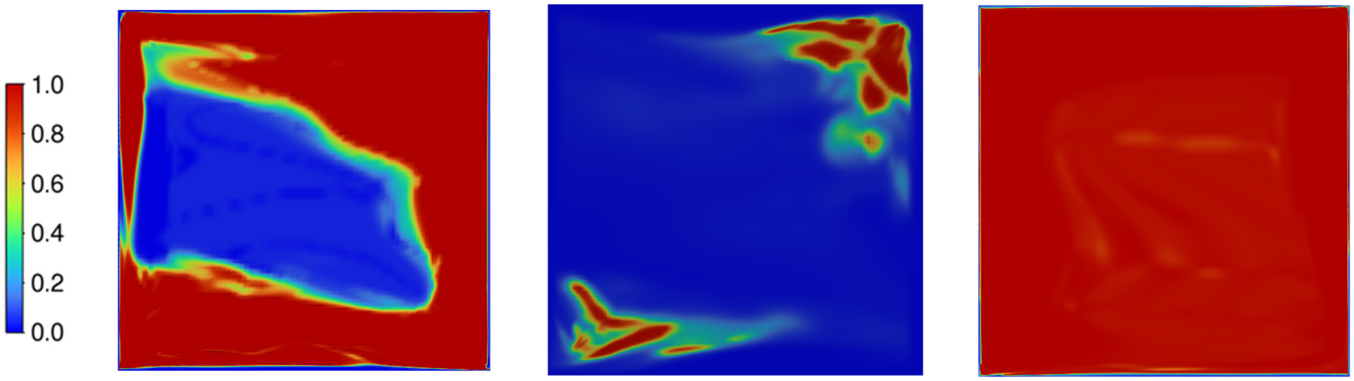
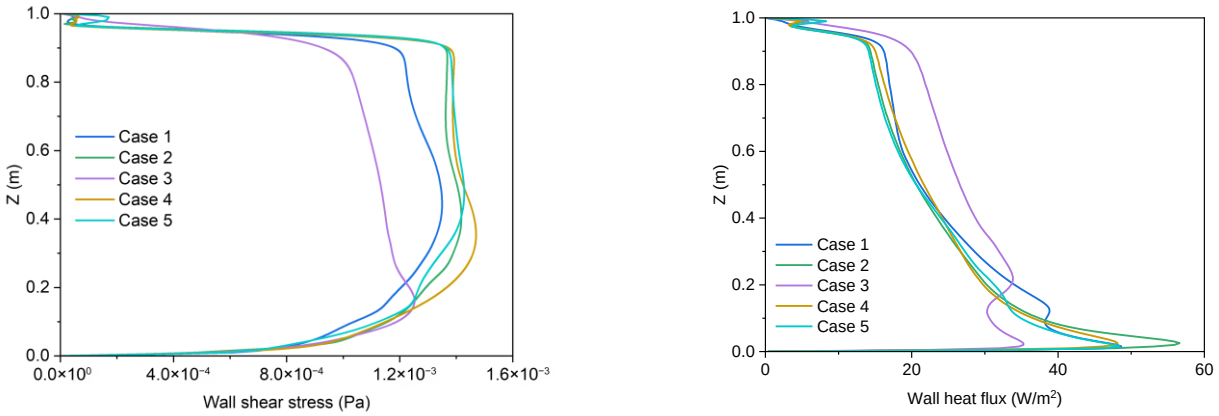


Figure 9. The contours of intermittency (γ) yielded from the correlation-based models in the Y = 0 plane: (**a**) Case 1; (**b**) Case 2; (**c**) Case 3.

As a result of the turbulence modelling methods, significantly different integral quantities are produced on the walls. Figure 10 shows the distributions of the predicted wall shear stress and heat flux on the hot wall. It was observed that both the wall shear stress and heat flux were very low in the lower and upper corners due to the small local w-velocity

component. The integral quantities quickly increased as the w-velocity built up along the height. The γ-Re_θ model produced the lowest wall shear stress but the highest wall heat flux. Again, the γ transport equation (Case 2) and low-*Re* modification (Case 5) produced very close simulations, in both wall shear stress and heat flux.



(**a**) (**b**)

Figure 10. The shear stress and heat flux on the hot wall: (**a**) wall shear stress; (**b**) wall heat flux.

Overall, for the low-speed natural convective flows of this study, the γ transport equation and Wilcox's low-*Re* modification to the SST k-ω model accurately simulated the air velocity and temperature fields. Analyses of the turbulence quantities revealed that the algebraic γ-equation and γ-Re_θ model overpredicted the air turbulence in the near-wall regions, while the k_l-k_t-ω model overpredicted that in the bulk region. Although Wilcox's low-*Re* modification did not explicitly model the laminar–turbulent transition, it had surprisingly good accuracy in velocity and temperature simulations. This attribute makes it a good option for engineering applications where the integral flow properties are the main quantities of interest, while the turbulence quantities are of secondary importance. In this study, Wilcox's model had a comparable accuracy with the γ transport equation for velocity and temperature simulations. However, it is worth noting that the turbulent viscosity yielded from the γ transport equation was one to four orders of magnitude higher than that predicted by the low-*Re* modification in the near-wall regions but three to four orders of magnitude lower in the bulk region, as shown in Figure 9. This difference, however, did not cause remarkable changes in the velocity and temperature simulations because of their very small magnitudes. Nevertheless, it is believed that the γ transport equation provided a more mechanistic modelling than the Wilcox's model. In particular, the difference in the predicted turbulence quantities and their effects on other flow properties may be amplified when the flow condition changes. Broad validation under various flow conditions including mixed and forced convective flows are still needed to further justify their suitability.

5. Conclusions

The natural convection flow of air in a differentially heated cavity (Ra = 1.5×10^9) was simulated using various transition turbulence models within the RANS framework. Comparison of the CFD results against the experimental and DNS data reported in the literature showed that the γ transport equation and Wilcox's low-*Re* modification to the SST k-ω model had good accuracy for the air velocity and temperature of the buoyancy-driven low-speed flows. Analyses of the turbulence quantities revealed that the accuracy of the two models stemmed from their effective modelling of turbulent quantities such as the turbulent kinetic energy and turbulent viscosity. By contrast, the algebraic γ-equation,

γ-Re_θ model and k_l-k_t-ω model either under- or overpredicted the turbulent quantities in different regions of the cavity, resulting in significant predictive errors for other flow field quantities. Comparatively, the γ transport equation offered more mechanistic modelling than the Wilcox model because it explicitly modelled the laminar–turbulent transition, although the Wilcox model can serve as an acceptable and cost-effective method to estimate laminar–turbulent transitions in engineering applications.

Author Contributions: Conceptualization, J.L. and X.L.; methodology, J.L. and X.L.; validation, X.L.; investigation, J.L. and X.L.; data curation, J.L.; writing—original draft preparation, J.L.; writing—review and editing, X.L.; funding acquisition, J.L. All authors have read and agreed to the published version of the manuscript.

Funding: This study is supported by the Sichuan Science and Technology Program (2023JDRC0033).

Institutional Review Board Statement: Not applicable.

Informed Consent Statement: Not applicable.

Data Availability Statement: The raw data supporting the conclusions of this article will be made available by the authors on request.

Conflicts of Interest: The authors declare no conflicts of interest.

References

1. Morkovin, M.V. Transition in open flow systems-a reassessment. *Bull. Am. Phys. Soc.* **1994**, *39*, 1882.
2. Jagadeesh, C.S.; Balthazar, M.; Gross, A.; Fasel, H.F. Experimental Investigation of the Structure and Dynamics of Laminar Separation Bubbles at the onset of Bursting. In Proceedings of the 31st AIAA Applied Aerodynamics Conference, San Diego, CA, USA, 24–27 June 2013.
3. Lemanov, V.V.; Lukashov, V.V.; Sharov, K.A.; Kh Abdrakhmanov, R. Laminar-turbulent transition in the near field of the jet at the instability regime of the jet source. *J. Phys. Conf. Ser.* **2018**, *1105*, 012015. [CrossRef]
4. Pope, S.B. *Turbulent Flows*; Cambridge University Press: Cambridge, UK, 2000.
5. Zakharov, V.E.; L'vov, V.S.; Falkovich, G. *Kolmogorov Spectra of Turbulence I: Wave Turbulence*; Springer: Berlin/Heidelberg, Germany, 2012.
6. Corrsin, S. *Investigation of Flow in an Axially Symmetric Heated Jet in Air*; California Institute of Technology: Pasadena, CA, USA, 1943.
7. Wilcox, D.C. Simulation of Transition with a Two-Equation Turbulence Model. *AIAA J.* **1994**, *32*, 247–255. [CrossRef]
8. Juntasaro, E.; Ngiamsoongnirn, K.; Thawornsathit, P.; Durbin, P. Development of an intermittency transport equation for modeling bypass, natural and separation-induced transition. *J. Turbul.* **2021**, *22*, 562–595. [CrossRef]
9. Mayle, R.E.; Schulz, A. *The Path to Predicting Bypass Transition*; American Society of Mechanical Engineers: New York, NY, USA, 1996.
10. Walters, D.; Cokljat, D. A Three-Equation Eddy-Viscosity Model for Reynolds-Averaged Navier–Stokes Simulations of Transitional Flow. *J. Fluids Eng.-Trans. Asme* **2008**, *130*, 121401. [CrossRef]
11. Shahbazi, A.A.; Esfahanian, V. Improving turbulence modeling for gas turbine blades: A novel approach to address flow transition and stagnation point anomalies. *J. Comput. Phys.* **2025**, *520*, 113499. [CrossRef]
12. Xu, J.; Jiang, X.; Wang, Y.; Dong, N.; Qiao, L.; Bai, J. Progress in local-variable-based transition-turbulence models for subsonic and transonic boundary layers. *Chin. J. Aeronaut.* **2025**, 103688. [CrossRef]
13. Zore, K.; Matyushenko, A.; Shah, S.; Aliaga, C.; Stokes, J.; Menter, F. Laminar-Turbulent Transition Prediction on Industrial CFD Applications. In Proceedings of the AIAA SCITECH 2022 Forum, San Diego, CA, USA, 3–7 January 2022.
14. Wu, L.; Xiao, Z. An improved four-equation transition-turbulence model for high-speed flows: Transition prediction and physical insight. *Int. J. Heat Mass Transf.* **2026**, *255*, 127798. [CrossRef]
15. Menter, F.R. Two-equation eddy-viscosity turbulence models for engineering applications. *AIAA J.* **1994**, *32*, 1598–1605. [CrossRef]
16. Ansys Inc. *Ansys Fluent Theory Guide*; Ansys Inc.: Canonsburg, PA, USA, 2023.
17. Menter, F.; Langtry, R.B.; Likki, S.; Suzen, Y.; Völker, S. A Correlation-Based Transition Model Using Local Variables—Part I: Model Formulation. *ASME J. Turbomach* **2006**, *128*, 413–422. [CrossRef]
18. Wilcox, D.C. *Turbulence Modeling for CFD*; DCW Industries: La Cañada, CA, USA, 2006.
19. Savill, A.M. Further progress in the turbulence modelling of by-pass transition. In *Engineering Turbulence Modelling and Experiments*; Rodi, W., Martelli, F., Eds.; Elsevier: Oxford, UK, 1993; pp. 583–592.

20. Rumsey, C.L. Apparent transition behavior of widely-used turbulence models. *Int. J. Heat Fluid Flow* **2007**, *28*, 1460–1471. [CrossRef]
21. Salat, J.; Xin, S.; Joubert, P.; Sergent, A.; Penot, F.; Le Quéré, P. Experimental and numerical investigation of turbulent natural convection in a large air-filled cavity. *Int. J. Heat Fluid Flow* **2004**, *25*, 824–832. [CrossRef]
22. Kitamura, K.; Mitsuishi, A.; Suzuki, T.; Misumi, T. Fluid flow and heat transfer of high-Rayleigh-number natural convection around heated spheres. *Int. J. Heat Mass Transf.* **2015**, *86*, 149–157. [CrossRef]
23. Celik, I.B.; Ghia, U.; Roache, P.J.; Freitas, C.J.; Coleman, H.; Raad, P.E. Procedure for Estimation and Reporting of Uncertainty Due to Discretization in CFD Applications. *J. Fluids Eng.* **2008**, *130*, 078001. [CrossRef]

Disclaimer/Publisher's Note: The statements, opinions and data contained in all publications are solely those of the individual author(s) and contributor(s) and not of MDPI and/or the editor(s). MDPI and/or the editor(s) disclaim responsibility for any injury to people or property resulting from any ideas, methods, instructions or products referred to in the content.